

Structure, Magnetic and Thermoelectric Properties of High Entropy Selenides $\text{Bi}_{0.6}\text{Sb}_{0.6}\text{In}_{0.4}\text{Cr}_{0.4}\text{Se}_3$

Feng Jiang^{1,2}, Tao Feng¹, Yongbin Zhu¹, Chengliang Xia², Chengyan Liu¹, Yue Chen^{2*} , and Weishu Liu^{1,3*} 

¹ Department of Materials Science and Engineering, Southern University of Science and Technology, Shenzhen 518055, Guangdong, China

² Department of Mechanical Engineering, The University of Hong Kong, Pokfulam Road, Hong Kong SAR, China

³ Guangdong Provincial Key Laboratory of Functional Oxide Materials and Devices, Southern University of Science and Technology, Shenzhen 518055, Guangdong, China

* Corresponding author, E-mail: yuechen@hku.hk; liuws@sustech.edu.cn

Abstract

Introducing magnetic elements or nanoparticles into the thermoelectric matrix is of great importance to regulate the thermoelectric performance and evaluate the magnetic-thermoelectric effect. While, the limitation of solid solution ability of magnetic elements in thermoelectric materials impedes the development of magnetic thermoelectric matrix. Herein, we have applied high entropy strategy to alloy a large amount of Cr elements into the Bi_2Se_3 sub-lattice, and successfully obtained a single-phase magnetic thermoelectric material in the nominal composition of $\text{Bi}_{0.6}\text{Sb}_{0.6}\text{In}_{0.4}\text{Cr}_{0.4}\text{Se}_3$. The Magnetization loop curves of $\text{Bi}_{0.6}\text{Sb}_{0.6}\text{In}_{0.4}\text{Cr}_{0.4}\text{Se}_3$ sample shows obvious ferromagnetic behavior with a coercivity of 2000 Oe and residual magnetization of 0.22 emu g^{-1} at 2 K. The temperature dependence of zero-field-cooled magnetic susceptibility and field-cooled magnetic susceptibility reveals a transition from ferromagnetism to paramagnetism at 61 K. These findings indicate that a magnetic Bi_2Se_3 based thermoelectric material is successfully obtained. The corresponding structure, magnetic and thermoelectric properties are also carefully discussed. This work offers a new avenue to achieve a magnetic thermoelectric material through high entropy strategy.

Key words: Selenides; Magnetic; High-entropy; Thermoelectric

Citation: Feng Jiang, Tao Feng, Yongbin Zhu, Chengliang Xia, Chengyan Liu, et al. Structure, Magnetic and Thermoelectric Properties of High Entropy Selenides $\text{Bi}_{0.6}\text{Sb}_{0.6}\text{In}_{0.4}\text{Cr}_{0.4}\text{Se}_3$. *Materials Lab* 2022, 1, 220045. DOI: [10.54227/mlab.20220045](https://doi.org/10.54227/mlab.20220045)

1 Introduction

Thermoelectric materials that can directly realize the conversion between heat and electricity via the Seebeck effect and Peltier effect have been explored to use in the Internet of Things (IoT).^[1–3] Conventional strategies, such as band engineering,^[4–6] nanostructure engineering,^[7,8] and defect engineering^[9,10] are commonly used to boost their thermoelectric performance, which was determined by the dimensionless figure of merit, ZT , termed as $ZT = S^2 \sigma T / \kappa$, where S , σ , T , and κ are Seebeck coefficient, electrical conductivity, absolute temperature, and thermal conductivity, respectively. Recently, introducing another dimensional discipline - magnetism into thermoelectrics attracted intensive attention. Many new phenomena like the quantum Hall effect,^[11] spin entropy,^[12,13] and magnetic-field dependent thermoelectric effect^[14,15] have been reported in the thermoelectric materials. These effects broaden widely practical applications of thermoelectric materials.

Generally, magnetic-thermoelectric materials can be divided into two categories. One is the intrinsic magnetic matrix, of which constituted composition contains at least one magnetism element, such as FeSb_2 ,^[16] MnTe ,^[17] MnBi_2Te_4 ,^[18] and so on. Another is a nonmagnetic matrix like classic Bi_2Te_3 -

based, Skutterudites, which can exhibit magnetic properties through magnetic doping^[19–21] or by introducing magnetic secondary phase or magnetic nanoparticles.^[22,23] These magnetic-thermoelectric materials exhibit magnetic-field dependent thermoelectric performance as compared with those improved by conventional strategies.^[23,24] Therefore, exploring and fabricating new magnetic-thermoelectric materials is of great significance. In recent years, some intrinsic thermoelectric materials with magnetic properties have been explored.^[13,25] However, the research on achieving a magnetic performance in conventional thermoelectric material family through doping is still a challenge due to the low solid solution ability.

Herein, we try to fabricate magnetic-thermoelectric material via high entropy strategy to go beyond the solid solution to stabilize a large amount of magnetic elements in the sub-lattice of non-magnetic thermoelectric materials. For the selection of magnetic element M in the formula of M_2Se_3 materials, we find that Cr_2Se_3 compound can form rhombohedral structure,^[26] which favors for stabilizing the similar structure of Bi_2Se_3 . Finally, a single phase with a formula of $\text{Bi}_{0.6}\text{Sb}_{0.6}\text{In}_{0.4}\text{Cr}_{0.4}\text{Se}_3$ is obtained. The crystal structure, magnetic properties, and thermoelectric properties of $\text{Bi}_{0.6}\text{Sb}_{0.6}\text{In}_{0.4}\text{Cr}_{0.4}\text{Se}_3$ sample were successfully obtained.

Received 12 June 2022; Accepted 16 July 2022; Published online

© 2022 The Author(s). *Materials Lab* published by Lab Academic Press

2 Materials and methods

2.1 Materials preparation

The raw powders were mixed thoroughly according to the stoichiometry ratio of Bi_2Se_3 , BiSbSe_3 , $\text{Bi}_{0.8}\text{Sb}_{0.8}\text{In}_{0.4}\text{Se}_3$ and $\text{Bi}_{0.6}\text{Sb}_{0.6}\text{In}_{0.4}\text{Cr}_{0.4}\text{Se}_3$ in a glove box and sealed in a quartz tube. The mixtures were heated to 1073 K for 10 h and soaked at this temperature for 48 h before furnace cooling to room temperature. As-fabricated ingots were crushed into fine powders and loaded into a graphite die. Then, the materials were condensed at 723 K for 5 min in a spark plasma sintering machine (SPS-211LX, Fuji Electronic Industrial Co. Ltd.) under a universal pressure of 40 MPa with a height of 7 mm for simultaneously measuring electrical and thermal properties along the direction perpendicular to the pressure direction.

2.2 Characterizations

The X-ray diffraction (XRD) patterns of the as-fabricated materials were collected using a Rigaku Smartlab diffractometer with a $\text{Cu K}\alpha$ radiation ($\lambda = 1.5406 \text{ \AA}$), and corresponding lattice constants were refined using Rietveld methods on the commercial software. The electrical resistivity and Seebeck coefficient were simultaneously measured by CTA (Cryo-all Thermoelectric Analysis, China). Thermal conductivity was obtained according to the equation, $\kappa = C_p D \rho$, where ρ is the density measured by Archimedeian method, C_p is for specific heat capacity measured by the differential scanning calorimeter (DSC, company), and D is the thermal diffusivity measured by the laser flash analyzer (LFA 467, Netzsch). The M-H curves of pristine Bi_2Se_3 , BiSbSe_3 , $\text{Bi}_{0.8}\text{Sb}_{0.8}\text{In}_{0.4}\text{Se}_3$ and $\text{Bi}_{0.6}\text{Sb}_{0.6}\text{In}_{0.4}\text{Cr}_{0.4}\text{Se}_3$ were measured with a MPMS (Quantum Design INC., USA) at 2 K. The magneto-Seebeck was measured adiabatically using the thermal transport option (TTO) on a

Quantum Design Physical Property Measurement System (PPMS 14 Tesla) with a one-heater and two-thermometer configuration. The low-temperature heat capacities were also performed by PPMS with logarithmic spacing in the temperature range of 2 K to 11 K in zero magnetic fields. The sample was mounted to the sample platform with a small amount of Apiezon grease. The uncertainty of the heat capacity measurement is about 3% in the low-temperature range.

3 Results and discussions

3.1 Crystal structure

Fig. 1 presents the XRD patterns of pristine $\text{Bi}_{0.8}\text{Sb}_{0.8}\text{Cr}_{0.4}\text{Se}_3$ and $\text{Bi}_{0.6}\text{Sb}_{0.6}\text{In}_{0.4}\text{Cr}_{0.4}\text{Se}_3$. In our previous work^[27] a single-phase $\text{Bi}_{0.8}\text{Sb}_{0.8}\text{In}_{0.4}\text{Se}_3$ was obtained. Once In is completely replaced by Cr, the obtained $\text{Bi}_{0.8}\text{Sb}_{0.8}\text{Cr}_{0.4}\text{Se}_3$ sample contains a small amount of secondary phase indexed as BiCrSe_3 , as shown in Fig. 1b. Therefore, it is difficult to stabilize a large amount of magnetic element Cr in the quaternary thermoelectric matrix. In order to improve the solid solubility and stabilize the magnetic element, we introduce Cr into the quaternary thermoelectric matrix $\text{Bi}_{0.8}\text{Sb}_{0.8}\text{In}_{0.4}\text{Se}_3$ to construct the high-entropy thermoelectric materials $\text{Bi}_{0.6}\text{Sb}_{0.6}\text{In}_{0.4}\text{Cr}_{0.4}\text{Se}_3$. The as-fabricated $\text{Bi}_{0.6}\text{Sb}_{0.6}\text{In}_{0.4}\text{Cr}_{0.4}\text{Se}_3$ still crystallizes in a rhombohedral structure, and no obvious purity phase was observed in these high-entropy thermoelectric materials. The refined lattice parameters for $\text{Bi}_{0.6}\text{Sb}_{0.6}\text{In}_{0.4}\text{Cr}_{0.4}\text{Se}_3$ and $\text{Bi}_{0.8}\text{Sb}_{0.8}\text{In}_{0.4}\text{Se}_3$ are $a = 4.050 \text{ \AA}$, $c = 28.826 \text{ \AA}$, and $a = 4.061 \text{ \AA}$, $c = 28.783 \text{ \AA}$ respectively, the ratio c/a is 7.12, slightly larger than 7.08 of $\text{Bi}_{0.8}\text{Sb}_{0.8}\text{In}_{0.4}\text{Se}_3$. Noted that the lattice was moderately elongated by the lattice distortion compared to the pure Bi_2Se_3 ($a = 4.138 \text{ \AA}$, $c = 28.640 \text{ \AA}$, with $c/a = 6.97$).

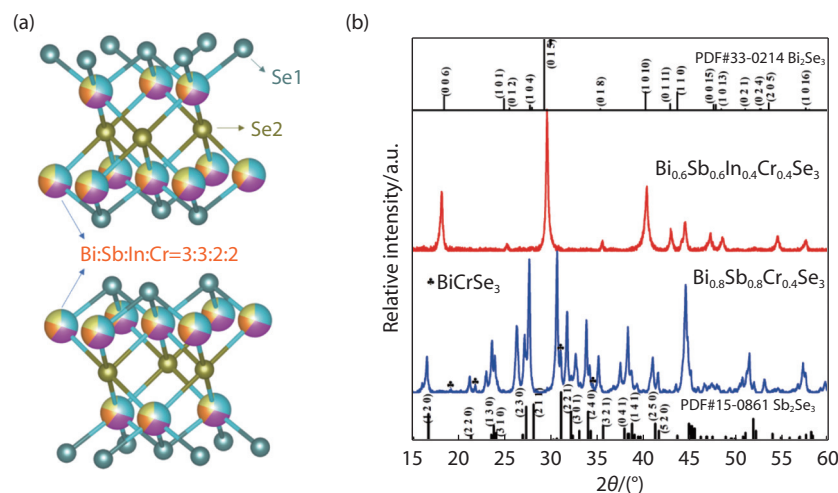


Fig. 1 (a) Crystal structure of the as-fabricated $\text{Bi}_{0.6}\text{Sb}_{0.6}\text{In}_{0.4}\text{Cr}_{0.4}\text{Se}_3$ high entropy selenides. Cyan for Se1, Brown for Se2, Mixed color for randomly distributed Bi, Sb, In, and Cr. (b) XRD patterns of pristine $\text{Bi}_{0.8}\text{Sb}_{0.8}\text{Cr}_{0.4}\text{Se}_3$ and $\text{Bi}_{0.6}\text{Sb}_{0.6}\text{In}_{0.4}\text{Cr}_{0.4}\text{Se}_3$. The insert symbol represented the secondary phase BiCrSe_3 (PDF#51-0750) in $\text{Bi}_{0.8}\text{Sb}_{0.8}\text{Cr}_{0.4}\text{Se}_3$ material.

3.2 Magnetic properties

Fig. 2 shows the magnetic M-H curves of the as-fabricated Bi_2Se_3 , BiSbSe_3 , $\text{Bi}_{0.8}\text{Sb}_{0.8}\text{In}_{0.4}\text{Se}_3$, and $\text{Bi}_{0.6}\text{Sb}_{0.6}\text{In}_{0.4}\text{Cr}_{0.4}\text{Se}_3$, respectively. All the Bi_2Se_3 , BiSbSe_3 , $\text{Bi}_{0.8}\text{Sb}_{0.8}\text{In}_{0.4}\text{Se}_3$ shows the diamagnetic behavior. The magnetization is relatively low,

and there is almost no hysteresis loop (Fig. 2a-2c). Instead, the M-H curve of $\text{Bi}_{0.6}\text{Sb}_{0.6}\text{In}_{0.4}\text{Cr}_{0.4}\text{Se}_3$ sample shows an obvious hysteresis loop and has a two order increment on magnetic moment, which is ascribed to the introduction of Cr element into the thermoelectric matrix (Fig. 2d). The residual magnet-

ization (M_r) and coercivity (H_c) of $\text{Bi}_{0.6}\text{Sb}_{0.6}\text{In}_{0.4}\text{Cr}_{0.4}\text{Se}_3$ material at 2 K are 0.22 emu g^{-1} and 2000 Oe, respectively, showing strong ferromagnetic behavior, of which value is comparable

to other reported magnetic materials of $\text{Mn}(\text{Bi}_x\text{Sb}_{1-x})_6\text{Te}_{10}$ [18] and $\text{Ti}_{0.25}\text{Zr}_{0.25}\text{Hf}_{0.50}\text{NiFe}_x\text{Sn}_{0.975}\text{Sb}_{0.025}$ [28]

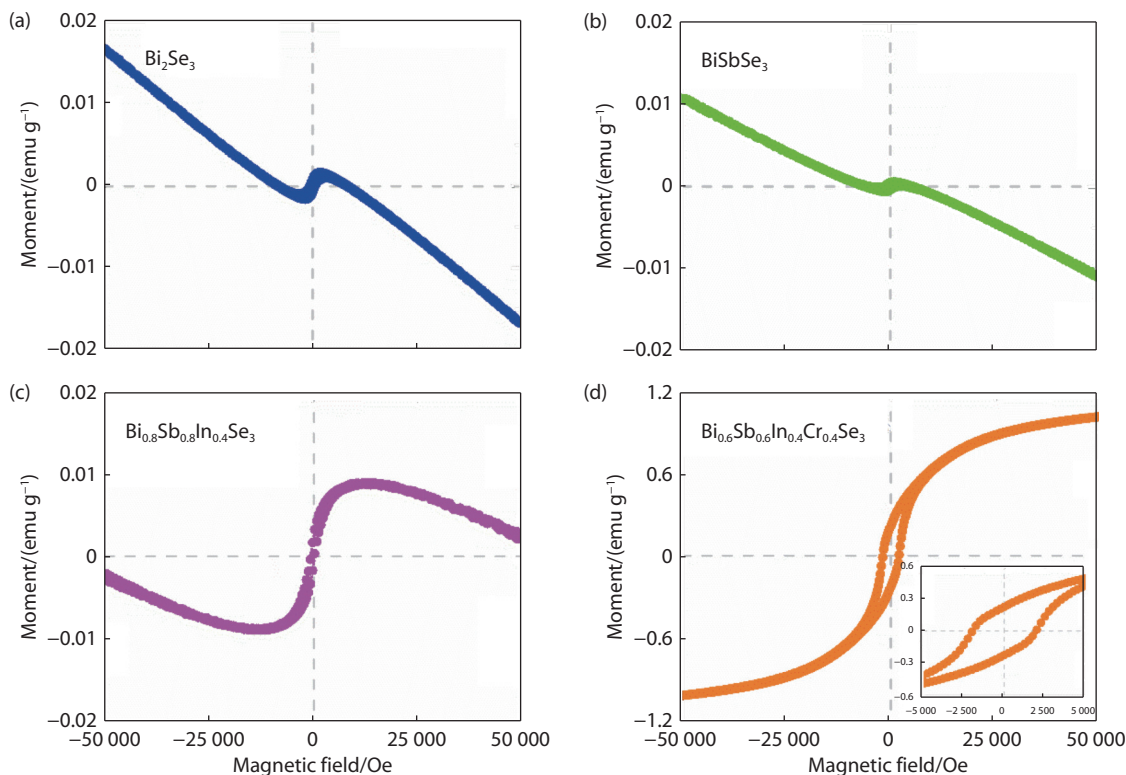


Fig. 2 M-H curves of (a) Bi_2Se_3 , (b) BiSbSe_3 , (c) $\text{Bi}_{0.8}\text{Sb}_{0.8}\text{In}_{0.4}\text{Se}_3$, and (d) $\text{Bi}_{0.6}\text{Sb}_{0.6}\text{In}_{0.4}\text{Cr}_{0.4}\text{Se}_3$ at 2 K.

The Curie point is determined through measuring magnetic M-T curves under the condition of zero-field cooling (ZFC) and field cooling (FC) at 1000 Oe. Fig. 3a shows the transition temperature from ferromagnetism to paramagnetism near 61 K in the $\text{Bi}_{0.6}\text{Sb}_{0.6}\text{In}_{0.4}\text{Cr}_{0.4}\text{Se}_3$ material, which is larger than that of 13.2 K in $\text{Mn}(\text{Bi}_x\text{Sb}_{1-x})_6\text{Te}_{10}$ [18]. This is further verified by measuring M-H curves at different temperature as shown in Fig. 3b. When the temperature increases from 2 K to 50 K, both magnetic moment and the area of hysteresis loop de-

creases. It is known that ferromagnetic materials have strong magnetism after being magnetized at low temperature. With increasing temperature, the magnetic domains and moment would be strongly affected by the intensification of lattice vibration [29]. When the temperature above the Curie temperature, the magnetic domain is collapsed and the average magnetic moment becomes zero, then the ferromagnetic substance changes into a paramagnetic substance.

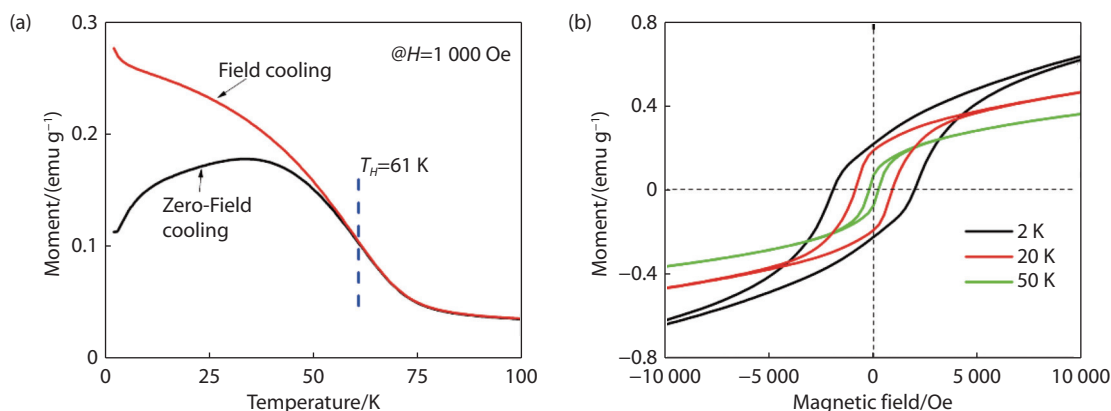


Fig. 3 (a) Zero-Field cooling and Field cooling curves of pristine $\text{Bi}_{0.6}\text{Sb}_{0.6}\text{In}_{0.4}\text{Cr}_{0.4}\text{Se}_3$ with a magnetization of 1000 Oe. (b) M-H curves of pristine $\text{Bi}_{0.6}\text{Sb}_{0.6}\text{In}_{0.4}\text{Cr}_{0.4}\text{Se}_3$ at different temperatures (2 K, 20 K and 50 K).

3.3 Low temperature heat capacity

The heat capacity of a substance below about $T = 10$ K is generally fit to theoretical functions, which may provide important information about the lattice, electronic and magnetic properties of a material as shown in Fig. 4. The low temperature heat capacity of $\text{Bi}_{0.8}\text{Sb}_{0.8}\text{In}_{0.4}\text{Se}_3$ sample were fitted to the following equation,^[30]

$$C_{m,p} = \gamma T + B_3 T^3 + B_5 T^5 + B_7 T^7 \quad (1)$$

where the γ is the Sommerfeld coefficient and the γT term represents the contribution of electronic heat capacity; the odd-powers in temperature ($B_3 T^3 + B_5 T^5 + B_7 T^7$) stands for the lattice vibration contribution to heat capacity^[31]. While, for

$\text{Bi}_{0.6}\text{Sb}_{0.6}\text{In}_{0.4}\text{Cr}_{0.4}\text{Se}_3$ sample, the term of ferromagnetism needs to be included as follows,

$$C_{m,p} = \gamma T + B_3 T^3 + B_5 T^5 + B_{\text{asw}} T^{1.5} e^{-\Delta/T} \quad (2)$$

Here, the $B_{\text{asw}} T^{1.5} e^{-\Delta/T}$ term stands for the magnetic contribution in the heat capacity^[32]. In the magnetic expression, the $B_{\text{asw}} T^{1.5}$ is the typical dependence of heat capacity with temperature for ferromagnets. The detailed fitting parameters are shown in Table 1. The root-mean-square (RMS) deviations for $\text{Bi}_{0.8}\text{Sb}_{0.8}\text{In}_{0.4}\text{Se}_3$ and $\text{Bi}_{0.6}\text{Sb}_{0.6}\text{In}_{0.4}\text{Cr}_{0.4}\text{Se}_3$ are 0.7017% and 0.4628%, respectively, indicating the fitting data coincide well with the experimental data. These results further confirm the existence of ferromagnetism in $\text{Bi}_{0.6}\text{Sb}_{0.6}\text{In}_{0.4}\text{Cr}_{0.4}\text{Se}_3$ sample as revealed by hysteresis loop.

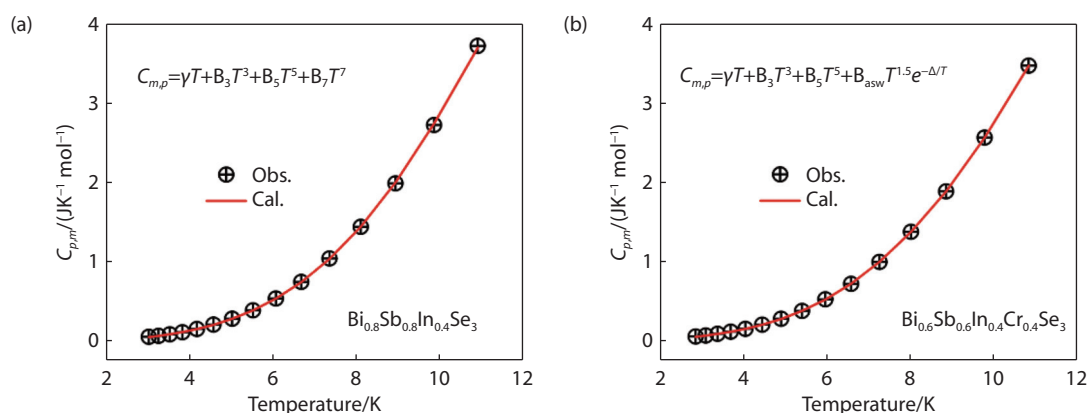


Fig. 4 Heat capacity of (a) $\text{Bi}_{0.8}\text{Sb}_{0.8}\text{In}_{0.4}\text{Se}_3$ and (b) $\text{Bi}_{0.6}\text{Sb}_{0.6}\text{In}_{0.4}\text{Cr}_{0.4}\text{Se}_3$ as a function of temperature over the range of 3 to 11 K. The dots stand for the experimental data, and the red line represents the fitted result.

Table 1. Fitting parameters of the heat capacity of $\text{Bi}_{0.8}\text{Sb}_{0.8}\text{In}_{0.4}\text{Se}_3$ and $\text{Bi}_{0.6}\text{Sb}_{0.6}\text{In}_{0.4}\text{Cr}_{0.4}\text{Se}_3$ below $T < 11$ K.

Compounds	Parameters	values
$\text{Bi}_{0.8}\text{Sb}_{0.8}\text{In}_{0.4}\text{Se}_3$	$\gamma/\text{J}\cdot\text{mol}^{-1}\cdot\text{K}^{-2}$	$6.6389\cdot 10^{-5}$
	$B_3/\text{J}\cdot\text{mol}^{-1}\cdot\text{K}^{-4}$	$1.7395\cdot 10^{-3}$
	$B_5/\text{J}\cdot\text{mol}^{-1}\cdot\text{K}^{-6}$	$2.1553\cdot 10^{-5}$
	$B_7/\text{J}\cdot\text{mol}^{-1}\cdot\text{K}^{-8}$	$-1.0218\cdot 10^{-7}$
	RMS%	0.7017
$\text{Bi}_{0.6}\text{Sb}_{0.6}\text{In}_{0.4}\text{Cr}_{0.4}\text{Se}_3$	$\gamma/\text{J}\cdot\text{mol}^{-1}\cdot\text{K}^{-2}$	$2.0651\cdot 10^{-3}$
	$B_3/\text{J}\cdot\text{mol}^{-1}\cdot\text{K}^{-4}$	$2.1751\cdot 10^{-3}$
	$B_5/\text{J}\cdot\text{mol}^{-1}\cdot\text{K}^{-6}$	$-5.4022\cdot 10^{-6}$
	$B_{\text{asw}}/\text{mol}$	0.4385
	Δ/K	25.4386
	RMS%	0.4628

According to the low-temperature fitting, the Sommerfeld coefficient γ are $6.6389\cdot 10^{-5} \text{ J}\cdot\text{mol}^{-1}\cdot\text{K}^{-2}$ and $2.0651\cdot 10^{-3} \text{ J}\cdot\text{mol}^{-1}\cdot\text{K}^{-2}$ for $\text{Bi}_{0.8}\text{Sb}_{0.8}\text{In}_{0.4}\text{Se}_3$ and $\text{Bi}_{0.6}\text{Sb}_{0.6}\text{In}_{0.4}\text{Cr}_{0.4}\text{Se}_3$, respectively. Then, the renormalized density of states at the Fermi level $N(E_F)$ can be deduced using the relation $\gamma = (\pi^2/3) k_B^2 N(E_F)$ ^[33]. Compared with $\text{Bi}_{0.8}\text{Sb}_{0.8}\text{In}_{0.4}\text{Se}_3$ sample, $\text{Bi}_{0.6}\text{Sb}_{0.6}\text{In}_{0.4}\text{Cr}_{0.4}\text{Se}_3$ shows an increased $N(E_F)$, which is consistent with the increased carrier concentration. Furthermore, the γ can also reflect the change of electron effective mass. In Fermi liquid model, γ can be expressed by the relation $\gamma = (m^*/m_B) \gamma^0$, where m_B and γ^0 represent the respective values for a non-interacting electron system^[34]. Generally, the increase of γ can be ascribed to the enhancement of the ef-

fective mass m^* of correlated electrons, indicating a higher m^* is obtained in the as-fabricated high entropy magnetic thermoelectric materials $\text{Bi}_{0.6}\text{Sb}_{0.6}\text{In}_{0.4}\text{Cr}_{0.4}\text{Se}_3$ sample in this work.

3.4 Thermoelectric properties

Fig. 5 presents the thermoelectric properties of pristine $\text{Bi}_{0.8}\text{Sb}_{0.8}\text{In}_{0.4}\text{Se}_3$ and $\text{Bi}_{0.6}\text{Sb}_{0.6}\text{In}_{0.4}\text{Cr}_{0.4}\text{Se}_3$. The electrical conductivity of both $\text{Bi}_{0.8}\text{Sb}_{0.8}\text{In}_{0.4}\text{Se}_3$ and $\text{Bi}_{0.6}\text{Sb}_{0.6}\text{In}_{0.4}\text{Cr}_{0.4}\text{Se}_3$ increases with temperature, while the absolute Seebeck coefficient decreases with temperature, exhibiting intrinsic semiconductor behavior. The electrical conductivity of $\text{Bi}_{0.6}\text{Sb}_{0.6}\text{In}_{0.4}\text{Cr}_{0.4}\text{Se}_3$ shown in Fig. 5a is 50 S m^{-1} at RT and increases to 250 S m^{-1} at 673 K. It is worth noting that the value of Seebeck coefficient for $\text{Bi}_{0.6}\text{Sb}_{0.6}\text{In}_{0.4}\text{Cr}_{0.4}\text{Se}_3$ is positive ($520 \mu\text{V K}^{-1}$ to $200 \mu\text{V K}^{-1}$) from RT to 673 K (Fig. 5b), further supporting that the increased configurational entropy can suppress the intrinsic Se vacancy of Bi_2Se_3 -based materials.^[27] To evaluate the effect of Cr alloying on the effective mass, Hall measurement was conducted. As listed in Table 2, the carrier concentration of high-entropy thermoelectric matrix $\text{Bi}_{0.6}\text{Sb}_{0.6}\text{In}_{0.4}\text{Cr}_{0.4}\text{Se}_3$ is $1.18\cdot 10^{18} \text{ cm}^{-3}$, which is an order larger than that of $\text{Bi}_{0.8}\text{Sb}_{0.8}\text{In}_{0.4}\text{Se}_3$. Based on the single parabolic band model, the effective mass for $\text{Bi}_{0.8}\text{Sb}_{0.8}\text{In}_{0.4}\text{Se}_3$ and $\text{Bi}_{0.6}\text{Sb}_{0.6}\text{In}_{0.4}\text{Cr}_{0.4}\text{Se}_3$, obtained through the Pisarenko relationship is 0.55 and 2.28, respectively, indicating that alloying Cr element can significantly increase the whole band effective mass. The enhanced effective mass might be contributed

to the magnetic drag effect induced by the magnetic Cr element in the matrix, which is also observed in other magnetic

materials, CuFeS_2 ,^[25] and $\text{CuGa}_{1-x}\text{Mn}_x\text{Te}_2$,^[21] Cr-doped Bi_2S_3 .

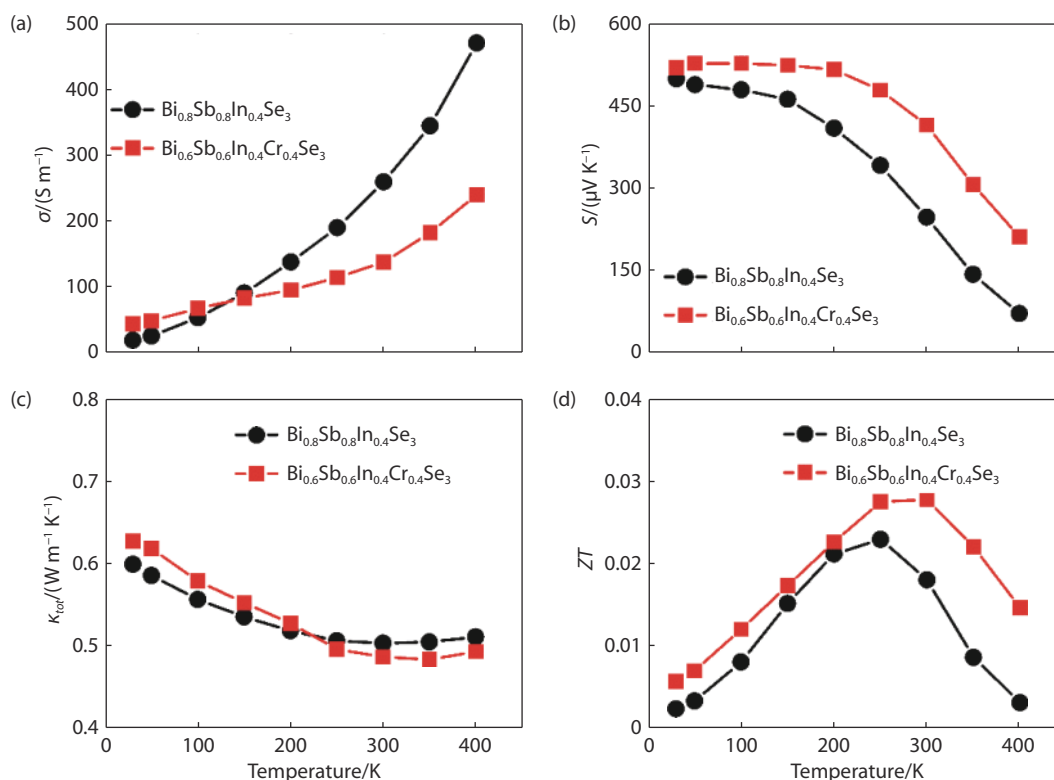


Fig. 5 Temperature dependent thermoelectric properties of $\text{Bi}_{0.8}\text{Sb}_{0.8}\text{In}_{0.4}\text{Se}_3$ and $\text{Bi}_{0.6}\text{Sb}_{0.6}\text{In}_{0.4}\text{Cr}_{0.4}\text{Se}_3$ samples: (a) electrical conductivity, (b) Seebeck coefficient, (c) thermal conductivity, and (d) ZT.

Table 2. Comparison of room-temperature electrical properties of $\text{Bi}_{0.6}\text{Sb}_{0.6}\text{In}_{0.4}\text{Cr}_{0.4}\text{Se}_3$ with $\text{Bi}_{0.8}\text{Sb}_{0.8}\text{In}_{0.4}\text{Se}_3$.

Compounds	S ($\mu\text{V K}^{-1}$)	σ (S m^{-1})	n (10^{18} cm^{-3})	μ ($\text{cm}^2 \text{ V}^{-1} \text{ s}^{-1}$)	m^*
$\text{Bi}_{0.8}\text{Sb}_{0.8}\text{In}_{0.4}\text{Se}_3$	500	18.10	0.17	5.88	0.55
$\text{Bi}_{0.6}\text{Sb}_{0.6}\text{In}_{0.4}\text{Cr}_{0.4}\text{Se}_3$	520	43.26	1.18	2.28	2.28

As compared with $\text{Bi}_{0.8}\text{Sb}_{0.8}\text{In}_{0.4}\text{Se}_3$, $\text{Bi}_{0.6}\text{Sb}_{0.6}\text{In}_{0.4}\text{Cr}_{0.4}\text{Se}_3$ possesses a comparable low thermal conductivity of $0.63 \text{ W m}^{-1} \text{ K}^{-1}$ at RT and $0.48 \text{ W m}^{-1} \text{ K}^{-1}$ at 623 K, as shown in Fig. 5c. Owing to the increased effective band mass (high Seebeck coefficient) and lower thermal conductivity at high temperatures, the dimensionless figure of merit ZT of $\text{Bi}_{0.6}\text{Sb}_{0.6}\text{In}_{0.4}\text{Cr}_{0.4}\text{Se}_3$ is about 4 times higher than that of $\text{Bi}_{0.8}\text{Sb}_{0.8}\text{In}_{0.4}\text{Se}_3$ at 673 K (Fig. 5d), showing promising thermoelectric performance with the introduction of magnetism. However, the ZT value is still quite low. Further optimization of carrier concentration and comprise of band flatten and carrier mobility, through adjunction of cationic elemental ratio, would be applied to improve the overall thermoelectric performance of high entropy selenides.

The magneto-Seebeck effect was also measured at 0, 3, and 9 Tesla in the low temperature range, as shown in Fig. 6. The Seebeck coefficients of the $\text{Bi}_{0.6}\text{Sb}_{0.6}\text{In}_{0.4}\text{Cr}_{0.4}\text{Se}_3$ sample under remains almost unchanged, indicating a weak response to the magnetic field. This may be attributed to the low mobility of $2.28 \text{ cm}^2 \text{ V}^{-1} \text{ s}^{-1}$ in the $\text{Bi}_{0.6}\text{Sb}_{0.6}\text{In}_{0.4}\text{Cr}_{0.4}\text{Se}_3$

sample.^[15,36,37] Therefore, improving the mobility of carriers in high entropy magnetic thermoelectric matrix and enhancing the magneto-Seebeck effect will be one of our future works.

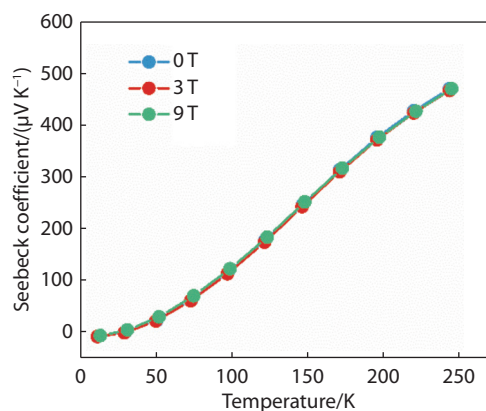


Fig. 6 The Magneto-Seebeck coefficient of $\text{Bi}_{0.6}\text{Sb}_{0.6}\text{In}_{0.4}\text{Cr}_{0.4}\text{Se}_3$ at 0, 3, and 9 Tesla in a temperature range of 2 K - 250 K.

4 Conclusions

In summary, we successfully applied high entropy strategy to achieve a single-phase thermoelectric matrix with magnetism in $\text{Bi}_{0.6}\text{Sb}_{0.6}\text{In}_{0.4}\text{Cr}_{0.4}\text{Se}_3$. The as-obtained high entropy thermoelectric matrix possesses an intrinsic positive Seebeck coefficient value of $\sim 520 \mu\text{V K}^{-1}$ and an ultralow thermal conductivity of $\sim 0.63 \text{ W m}^{-1} \text{ K}^{-1}$ at room temperature. $\text{Bi}_{0.6}\text{Sb}_{0.6}\text{In}_{0.4}\text{Cr}_{0.4}\text{Se}_3$ shows an obvious hysteresis loop and strong ferromagnetic behavior when temperature below 61 K. Its magnetization is two orders of magnitude higher than that of those thermoelectric matrix without magnetic element Cr at 2 K. Besides, the effective mass of $\text{Bi}_{0.6}\text{Sb}_{0.6}\text{In}_{0.4}\text{Cr}_{0.4}\text{Se}_3$ is also greatly enhanced through the introduction of magnetic elements, and thus increasing about 4 times ZT value at 673 K as compared with pristine $\text{Bi}_{0.8}\text{Sb}_{0.8}\text{In}_{0.4}\text{Se}_3$. These findings provide a new route for obtaining a magnetic thermoelectric matrix through a high-entropy strategy and highlight the great potential of magnetic element doped selenides matrix for thermoelectric energy conversion.

Acknowledgments

This work was supported by the financial aid from the National Key Research and Development Program of China (2018YFB0703600), and Guangdong Provincial Key Laboratory Program (2021B1212040001), Shenzhen Key Program for Long-Term Academic Support Plan (20200925164021002).

Conflict of interest

The authors declare no conflict of interest.

Author contributions

F. Jiang and W. S. Liu proposed the research direction and design this work. T. Feng performed the measurement of low heat capacity and polish the manuscript. C. L. Xia, C. Y. Liu, Y. Chen and W. S. Liu joined the discussion and gave useful suggestions. F. Jiang and T. Feng are equal to this work.

REFERENCES

1. R. P. Chasmar and R. Stratton, *J. Electro. Control*, 1959, 7, 52
2. J. He and T. M. Tritt, *Science*, 2017, 357, eaak9997
3. W. S. Liu, X. Qian, C.-G. Han, Q. K. Li and G. Chen, *Appl. Phys. Lett.*, 2021, 118, 020501
4. Y. Z. Pei, X. Y. Shi, A. LaLonde, H. Wang, L. D. Chen and G. J. Snyder, *Nature*, 2011, 473, 66
5. H. L. Yu, A. R. Shaikh, F. Xiong and Y. Chen, *ACS Appl. Mater. Interfaces*, 2018, 10, 9889
6. H. Usui and K. Kuroki, *J. Appl. Phys.*, 2017, 121, 165101
7. B. Poudel, Q. Hao, Y. Ma, Y. C. Lan, A. Minnich, B. Yu, X. Yan, D. Z. Wang, A. Muto, D. Vashaee, X. Y. Chen, J. M. Liu, M. S. Dressel, G. Chen and Z. F. Ren, *Science*, 2008, 320, 634
8. W. S. Liu, X. Yan, G. Chen and Z. F. Ren, *Nano Energy*, 2012, 1, 42
9. T. J. Zhu, L. P. Hu, X. B. Zhao and J. He, *Adv. Sci.*, 2016, 3, 1600004
10. J. Li, S. Zhang, F. Jia, S. Q. Zheng, X. L. Shi, D. Q. Jiang, S. Y. Wang, G. W. Lu, L. M. Wu and Z.-G. Chen, *Mater. Today Phys.*, 2020, 15, 100269
11. T. Zhao, K. Zhao, Q. Y. Liu, X. S. Yang and Y. Zhao, *J. Appl. Phys.*,

- 2020, 127, 155101
12. P. J. Sun, K. R. Kumar, M. Lyu, Z. Wang, J. S. Xiang and W. Q. Zhang, *The Innovation*, 2021, 2, 100101
13. S. Hébert, R. Daou, A. Maignan, S. Das, A. Banerjee, Y. Klein, C. Bourges, N. Tsujii and T. Mori, *Sci. Tech. Adv. Mater.*, 2021, 22, 583
14. J. K. Furdyna, *J. Appl. Phys.*, 1988, 64, R29
15. T. Feng, P. S. Wang, Z. J. Han, L. Zhou, W. Q. Zhang, Q. H. Liu and W. S. Liu, *Adv. Mater.*, 2022, 34, 2200931
16. A. Bentien, S. Johnsen, G. K. H. Madsen, B. B. Iversen and F. Steglich, *EPL*, 2007, 80, 17008
17. Y. Zheng, T. Lu, M. M. H. Polash, M. Rasoulianboroujeni, N. Liu, M. E. Manley, Y. Deng, P. J. Sun, X. L. Chen, R. P. Hermann, D. Vashaee, J. P. Heremans and H. Zhao, *Sci. Adv.*, 2019, 5, 9461
18. J. Z. Wu, F. C. Liu, C. Liu, Y. Wang, C. C. Li, Y. F. Lu, S. Matsuishi and H. Hosono, *Adv. Mater.*, 2020, 32, 2001815
19. T. Okuda, N. Jufuku, S. Hidaka and N. Terada, *Phys. Rev. B*, 2005, 72, 144403
20. Z. C. Wei, C. Y. Wang, J. Y. Zhang, J. Yang, Z. L. Li, Q. D. Zhang, P. F. Luo, W. Q. Zhang, E. K. Liu and J. Luo, *ACS Appl. Mater. Interfaces*, 2020, 12, 20653
21. F. Ahmed, N. Tsujii and T. Mori, *J. Mater. Chem. A*, 2017, 5, 7545
22. W. Y. Zhao, Z. Y. Liu, P. Wei, Q. J. Zhang, W. T. Zhu, X. L. Su, X. F. Tang, J. H. Yang, Y. Liu, J. Shi, Y. M. Chao, S. Q. Lin and Y. Z. Pei, *Nat. Nanotechnology*, 2017, 12, 55
23. W. Y. Zhao, Z. Y. Liu, Z. G. Sun, Q. J. Zhang, P. Wei, X. Mu, H. Y. Zhou, C. C. Li, S. F. Ma, D. Q. He, P. X. Ji, W. T. Zhu, X. L. Nie, X. L. Su, X. F. Tang, B. G. Shen, X. L. Dong, J. H. Yang, Y. Liu and J. Shi, *Nature*, 2017, 549, 247
24. N. Jia, J. Cao, X. Y. Tan, J. F. Dong, H. F. Liu, C. K. I. Tan, J. W. Xu, Q. Y. Yan, X. J. Loh and A. Suwardi, *Mater. Today Phys.*, 2021, 21, 100519
25. H. Takaki, K. Kobayashi, M. Shimono, N. Kobayashi, K. Hirose, N. Tsujii and T. Mori, *Mater. Today Phys.*, 2017, 3, 85
26. D. Chen, F. Jiang, L. Fang, Y.-B. Zhu, C.-C. Ye and W.-S. Liu, *Rare Met.*, 2022, 41, 1543
27. F. Jiang, C. L. Xia, Y. B. Zhu, Z. J. Han, C. Y. Liu, J. T. Xia, Y. Chen and W. S. Liu, *Appl. Phys. Lett.*, 2021, 118, 193903
28. T. P. Bailer, R. Lu, P. F. P. Poudeu and C. Uher, *Mater. Today Phys.*, 2019, 11, 100155
29. F.-H. Sun, S. F. Ma, W. Y. Zhao, C. C. Li, X. H. Sang, P. Wei and Q. J. Zhang, *Rep. Prog. Phys.*, 2021, 84, 096501
30. T. Feng, L. Q. Li, Q. Shi, Y. L. Zhang and G. S. Li, *J. Chem. Thermodyn.*, 2020, 145, 106040
31. T. Feng, L. Q. Li, Q. Shi, X. L. Che, X. L. Xu and G. S. Li, *J. Chem. Thermodyn.*, 2018, 119, 127
32. D. A. McQuarrie, *Statistical Mechanics*, University Science Books, USA, 2000.
33. Y. Tokura, Y. Taguchi, Y. Okada, Y. Fujishima, T. Arima, K. Kumagai and Y. Iye, *Phys. Rev. Lett.*, 1993, 70, 2126
34. D. Pines and P. Nozieres, *The Theory of Quantum Liquids*, W. A. Benjamin, USA, 1966.
35. R. Fortulan, S. A. Yamini, C. Nwanebu, S. W. Li, T. Baba, M. J. Reece and T. Mori, *ACS Appl. Energy Mater.*, 2022, 5, 3845
36. T. Teramoto, T. Komine, M. Kuraishi and R. Sugita, *J. Appl. Phys.*, 2008, 103, 043717
37. M. S. Akhanda, S. E. Rezaei, K. Esfarjani, S. Krylyuk, A. V. Davydov, and M. Zebarjadi, *Phys. Rev. Mater.*, 2021, 5, 015403



©2022 The Authors. *Materials Lab* is published by Lab Academic Press. This is an open access article under the terms of the Creative Commons Attribution License, which permits use, distribution and reproduction in any medium, provided the original work is properly cited.